OXFORD

Human Molecular Genetics, 2016, Vol. 25, No. 17 3729–3740

doi: 10.1093/hmg/ddw219
Advance Access Publication Date: 8 July 2016
Original Article

ORIGINAL ARTICLE

Calcium dynamics change in degenerating cone photoreceptors

Manoj Kulkarni[1,2,3], Dragana Trifunović[1], Timm Schubert[1,2], Thomas Euler[1,2,4,*] and François Paquet-Durand[1,*]

[1]Institute for Ophthalmic Research, [2]Werner Reichardt Centre for Integrative Neuroscience, [3]Graduate School of Cellular & Molecular Neuroscience and [4]Bernstein Centre for Computational Neuroscience, University of Tübingen, Tübingen, Germany

*To whom correspondence should be addressed at: Tel: +49 7071 29 87430; Fax: +49 7071 29 5777; Email: francois.paquet-durand@klinikum.uni-tuebingen.de(F.P-D.); Tel: +49 7071 29 85028; Fax: +49 7071 29 25011; Email: thomas.euler@cin.uni-tuebingen.de(T.E.)

Abstract

Cone photoreceptors (cones) are essential for high-resolution daylight vision and colour perception. Loss of cones in hereditary retinal diseases has a dramatic impact on human vision. The mechanisms underlying cone death are poorly understood, and consequently, there are no treatments available. Previous studies suggest a central role for calcium (Ca^{2+}) homeostasis deficits in photoreceptor degeneration; however, direct evidence for this is scarce and physiological measurements of Ca^{2+} in degenerating mammalian cones are lacking.

Here, we took advantage of the transgenic *HR2.1:TN-XL* mouse line that expresses a genetically encoded Ca^{2+} biosensor exclusively in cones. We cross-bred this line with mouse models for primary ("cone photoreceptor function loss-1", *cpfl1*) and secondary ("retinal degeneration-1", *rd1*) cone degeneration, respectively, and assessed resting Ca^{2+} levels and light-evoked Ca^{2+} responses in cones using two-photon imaging. We found that Ca^{2+} dynamics were altered in *cpfl1* cones, showing higher noise and variable Ca^{2+} levels, with significantly wider distribution than for wild-type and *rd1* cones. Unexpectedly, up to 21% of *cpfl1* cones still displayed light-evoked Ca^{2+} responses, which were larger and slower than wild-type responses. In contrast, genetically intact *rd1* cones were characterized by lower noise and complete lack of visual function.

Our study demonstrates alterations in cone Ca^{2+} dynamics in both primary and secondary cone degeneration. Our results are consistent with the view that higher (fluctuating) cone Ca^{2+} levels are involved in photoreceptor cell death in primary (*cpfl1*) but not in secondary (*rd1*) cone degeneration. These findings may guide the future development of therapies targeting photoreceptor Ca^{2+} homeostasis.

Introduction

Human vision depends primarily on cone photoreceptors, which mediate high-resolution, day-light colour vision. Rod photoreceptors (rods), on the other hand, are responsible for vision under dim-light conditions, *i.e.* at night. Cone loss can occur as a consequence of a mutation in the cone itself (*primary cone degeneration*) or as a "side-effect" of rod photoreceptor loss (*secondary cone degeneration*). A rapid cone loss as a consequence of mutations in cone-specific *Pde6c* (cGMP-specific phosphodiesterase) is present in the *cpfl1* mouse, an animal model for primary cone degeneration (1–3). Secondary cone degeneration, on the other hand, is observed as a consequence of primary rod photoreceptor cell death in diseases like Retinitis Pigmentosa (4,5). The *rd1* mouse carries a rod-specific *Pde6b* mutation and is a well-known model for

Received: May 10, 2016. **Revised:** June 24, 2016. **Accepted:** June 25, 2016

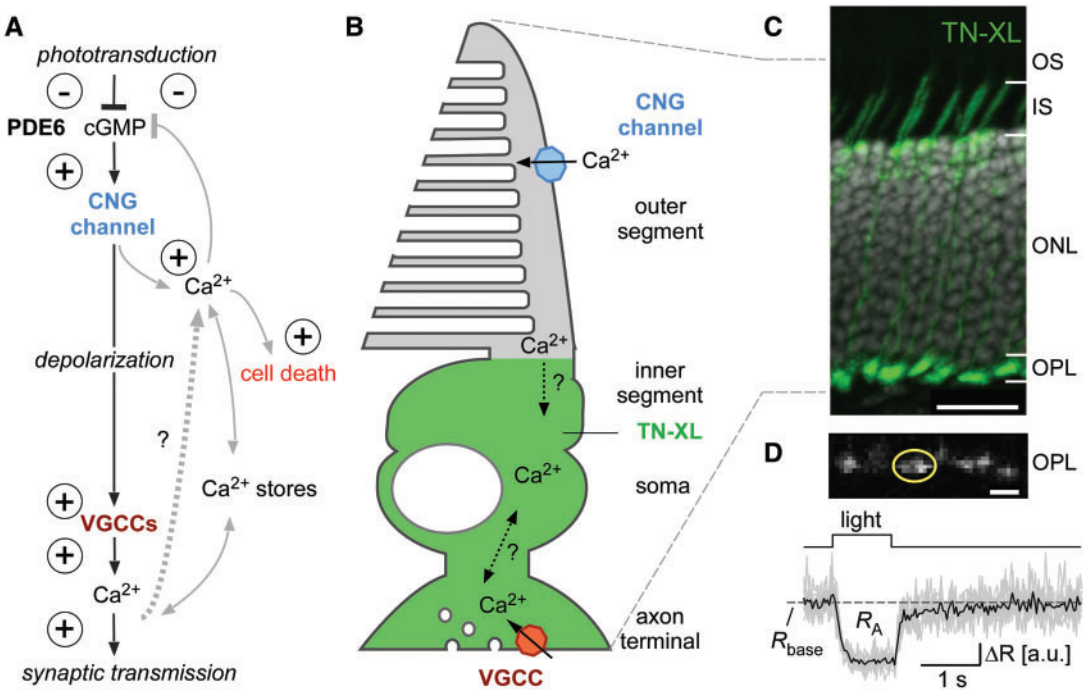

Figure 1. Photoreceptor Ca^{2+} signalling and experimental model. (**A**) The phototransduction cascade tightly regulates outer segment (OS) Ca^{2+} influx *via* cGMP-dependent cyclic nucleotide-gated (CNG) channels. Currents through CNG channels modulate the membrane potential and, thereby, voltage-gated Ca^{2+} channels (VGCCs) in the photoreceptor axon terminal and glutamate release. (**B**) Ca^{2+} is highly compartmentalized in healthy photoreceptors and diffusion is restricted between OS, inner segment (IS), soma, and axon terminal. (**C**) Vertical slice of a transgenic *HR2.1:TN-XL* mouse retina (outer retina shown), with cones selectively expressing the Ca^{2+} biosensor TN-XL (green; *cf.* green areas in (B); grey, photoreceptor nuclei stained with DAPI). (**D**) Ca^{2+} responses (bottom) to a 1-s light-flash recorded from a cone axon terminal (top; yellow circle) in a slice retinal preparation (mean, black trace; single trials, grey traces). Ca^{2+} signals shown as the change in ratio ($\Delta R = F_A/F_D$) of the acceptor fluorescence (F_A) to the donor fluorescence (F_D) (Methods). PDE6, phosphodiesterase 6; cGMP, 3'-5'-cyclic guanosine monophosphate; ONL, outer nuclear layer; OPL, outer plexiform layer. Scale bars: c, 20 μm; d, 5 μm.

secondary cone degeneration (6). We used *cpfl1* and *rd1* mouse lines to investigate the role of Ca^{2+} homeostasis in primary and secondary cone degeneration, respectively.

In the intact photoreceptor, Ca^{2+} has many important functions (Fig. 1A and B) , including modulating the transduction cascade in the outer segment (OS), and triggering the transmitter release from the axon terminals (7–9). In the dark, high cGMP levels in the OS activate cyclic nucleotide-gated (CNG) channels and allow for Ca^{2+} influx (10–12). In the light, Ca^{2+} levels drop due to cGMP hydrolysis by phosphodiesterase 6 (PDE6) and the subsequent closure of CNG channels. Low Ca^{2+} levels allow dissociation of Ca^{2+} from guanylate cyclase-activating proteins (GCAPs), disinhibition of guanylate cyclase (GC), restoring cGMP levels. This close coupling between cGMP and Ca^{2+} levels, together with the finding that mutant photoreceptors show an abnormal cGMP accumulation (13–15), led to the hypothesis of cGMP-mediated Ca^{2+} "overload" triggering degeneration (16).

Many studies support this "high Ca^{2+} hypothesis" (15,17–20), however, there are also several contradicting results: For instance, treatments with Ca^{2+} channel blockers, aimed at reducing Ca^{2+} overload and, thus, preventing or at least delaying photoreceptor degeneration, produced inconsistent results for primary rod degeneration (21–24). Furthermore, data from CNGA3-deficient mice show that in the absence of cone CNG channels (and CNG channel-mediated Ca^{2+} influx) cones still degenerate (25). Additionally, a functional study in *Pde6c*^{w59} mutant zebrafish found no increase in cone Ca^{2+} levels, but instead a suppression of (spontaneous) Ca^{2+} transients (26). Finally, also an alternative hypothesis has been promoted, which is based on the idea that photoreceptor death might be triggered by too low Ca^{2+} (i.e. the "low Ca^{2+} hypothesis") (27).

Here, we set out to study Ca^{2+} dynamics in degenerating cones using a transgenic mouse line (*HR2.1:TN-XL*) that expresses a genetically encoded ratiometric Ca^{2+} biosensor selectively in cones and allows monitoring of light-evoked Ca^{2+} signals in individual cone axon terminals (28–31). In healthy photoreceptors, opening of CNG channels in the dark depolarizes the cone membrane. Voltage-gated Ca^{2+} channels (VGCCs) in the synaptic terminal translate this depolarization into a Ca^{2+} influx, which in turn triggers synaptic vesicle fusion with the membrane and glutamate release (32–35). Thus, the presynaptic Ca^{2+} level in photoreceptors can serve as a proxy for upstream CNG channel activation in the OS (28).

To study cone Ca^{2+} in primary and secondary cone degeneration, we crossbred the *HR2.1:TN-XL* mouse line with the *cpfl1* and *rd1* PDE6 mutant lines, respectively. Ca^{2+} signals were compared between these *cpfl1* and *rd1* mutant crossbreds and the "wild-type" retina of *HR2.1:TN-XL* mice. We observed differential changes in Ca^{2+} in the two mutant lines: In primary cone degeneration, Ca^{2+} levels were more variable, noisy, and tended to be higher than in *wild-type* (*wt*). Notably, a substantial fraction of these cones showed robust light-evoked Ca^{2+} responses. On the other hand, in secondary cone degeneration, cone Ca^{2+} levels appeared to be lower and less variable compared to *wt* and did not show light-evoked Ca^{2+} responses. Our data are consistent with the idea of higher Ca^{2+} levels being involved in primary (*cpfl1*), but not in secondary (*rd1*) cone degeneration.

Materials and Methods

Animals

The transgenic mouse line *HR2.1:TN-XL* (C57BL/6J background) expresses the Ca^{2+} biosensor TN-XL (36) under the control of the human red opsin promoter (HR2.1) selectively in cone photoreceptors (28) (Fig. 1C). To study primary and secondary cone degeneration, we crossbred the biosensor line with the original *rd1* and *cpfl1* mutant animals to generate the *HR2.1:TN-XL* x *cpfl1* (C57BL/6J background) and *HR2.1:TN-XL* x *rd1* (C57BL/6J x C3H background) lines. Using PCR amplification and *NdeI* digestion, we verified that these lines were free of the *rd8* (*Crb1*) mutation (37). While a previous study on C3H *rd1* and congenic C3H *wt* animals, the latter of which show normal electroretinographic responses, had in principle ruled out the presence of the *Nob5* (*Gpr179*) mutation (38), we additionally performed a PCR-based analysis employed recently in a survey on C3H mouse lines (39). As shown in Supplementary Material, Figure S1, the *Nob5* mutation is absent in C3H *rd1* mice used in our study. For simplicity, in the later parts of the manuscript, we refer to the biosensor lines as *wt*, *cpfl1*, and *rd1*. For Ca^{2+} imaging experiments (see below), we used mice in two time windows (postnatal days 18-20 (P18-20) and P30-33), to which we refer to as P18+ and P30+, respectively. See results for a justification for the use of these time-frames. In general, we used mice irrespective of gender.

Prior to Ca^{2+} imaging, the mice were dark-adapted for approx. 2 hours and then anaesthetized using isoflurane (CP Pharma, Burgdorf, Germany). For immunostainings, we used P20 and P30 as analysis time points and the animals were anaesthetized with CO_2. In both cases, anaesthetized mice were killed by decapitation. All procedures were performed in accordance with the law on animal protection issued by the German Federal Government (Tierschutzgesetz) and approved by the institutional animal welfare committee of the University of Tübingen.

Immunohistochemistry and fluorescence microscopy

Eyes were marked on the nasal side prior to enucleation. They were fixed in 4% PFA in 0.1 M phosphate buffer saline (PBS, pH 7.4) (~1 hour) and cryo-protected in 30% sucrose in PBS at 4°C overnight. Then, eyes were embedded in Tissue-Tek OCT compound (Sakura Finetek Europe, Alphen aan Den Rijn, Netherlands) and stored at −20 °C until cryo-sectioning into 12 μm thick vertical sections. Sections were rehydrated with PBS, permeabilized in 0.1% Triton X-100 in PBS containing blocking solution (10% goat or donkey serum, 1% BSA). As primary antibodies, we used rabbit anti-GFP (1:600; Millipore, Darmstadt, Germany) or mouse anti-GFP (1:500; Abcam, Cambridge, UK); sheep anti-cGMP (1:500, from Harry W.M. Steinbusch, Maastricht University, Maastricht, Netherlands) and guinea pig anti-glycogen phosphorylase (1:1000, kind gift from B. Pfeiffer-Guglielmi, University of Tübingen, Tübingen, Germany). As secondary antibodies, we used Alexa Fluor 568 donkey anti-sheep (1:500; Invitrogen, Carlsbad, USA), Alexa Fluor 488 goat anti-rabbit (1:500; Molecular Probes, Eugene, USA), Alexa Fluor 488 goat anti-mouse (1:500; Molecular Probes) and FITC goat anti-guinea-pig (1:300; Sigma, Saint Louis, USA). The terminal deoxynucleotidyl transferase dUTP nick end labelling (TUNEL) assay (Roche Diagnostics, Mannheim, Germany) was performed using the TMR red kit as per manufacturer's instruction. Z-stack and mosaic images were captured on an Imager Z1 ApoTome microscope using a 20x air objective (0.8 NA; *cf.* Fig. 2A, *wt* and *cpfl1*) or a 63x oil immersion objective (1.4 NA; *cf.* Fig. 2A, *rd1*), and AxioVision (v.4.8.1.0) software (Carl Zeiss Microscopy GmbH, Oberkochen, Germany). Figures were assembled either in Adobe Photoshop CS5 (Adobe Systems, San Jose, USA) or Canvas 11 (ACD Systems International Inc., Seattle, USA).

Analysis of immunodata

The data were obtained from at least three different animals and for each animal at least three immunostained vertical sections were quantified, using mosaic images acquired at 20× magnification. For analysis, the area of the outer nuclear layer (ONL) and the length of the retinal sections were determined using the Zeiss Axiovision software. cGMP positive cells were counted in both biosensor and non-biosensor lines and were expressed as percent positive cells in the ONL (*rd1* retina), or as percent positive cones (*wt*, *rd1* and *cpfl1*). To estimate cone density (number of somata per 10 μm) for P20, P24 and P30 in both biosensor and non-biosensor lines, cones were labelled using glycogen phosphorylase (40) and counted in defined areas. Cones were only included if at least the inner segment (IS) and the soma could be clearly identified. To quantify dying cells, the *in situ* TUNEL assay was also performed on vertical sections (Supplementary Material, Fig. S2). We measured the area of the ONL, divided it by the total number of cells (obtained from DAPI staining) in that area and determined the fraction of TUNEL-positive nuclei (Supplementary Material, Fig. S3). Statistical comparisons were made using the Wilcoxon rank-sum test using IGOR Pro (Wavemetrics, Lake Oswego, USA).

Two-photon Ca^{2+} imaging

The preparation of retinal slices for Ca^{2+} imaging was performed as described previously (28,31). In brief, eyes were enucleated and dissected in carboxygenated (95% O_2, 5% CO_2) artificial cerebrospinal fluid (ACSF) solution, which contained (in mM): 125 NaCl, 2.5 KCl, 2 $CaCl_2$, 1 $MgCl_2$, 1.25 NaH_2PO_4, 26 $NaHCO_3$, 0.5 L-glutamine, and 20 glucose; maintained at pH 7.4 using carboxygen. Consecutive vertical slices (~200 μm thick) were cut using a tissue chopper (41) and then transferred to the recording chamber of a two-photon microscope, where they were constantly perfused with warmed (~37 °C) ACSF. The microscope (for details, see (42)), consisted of a customized MOM (movable objective microscope; designed by W. Denk, MPI of Neurobiology, Martinsried; purchased from Science Products/Sutter Instruments, Novato, USA), equipped with a mode-locked Ti:Sapphire laser (MaiTai-HP DeepSee; Newport Spectra-Physics, Darmstadt, Germany) tuned to 860 nm, two fluorescence detection channels (483 band-pass (BP) 32; 535 BP 50; AHF, Tübingen, Germany), and a 20x water-immersion objective (XLUMPlanFL, 0.95 NA; Olympus, Hamburg, Germany). The system was controlled by the image acquisition software ScanM (by M. Müller, MPI of Neurobiology, Martinsried, Germany, and T.E.) running under IGOR Pro 6.3, or CfNT (M. Müller, MPI, Martinsried, Germany). A custom-built dichromatic light stimulator (29), equipped with two band-pass filtered LEDs (UV filter: 360 BP 12; green: 578 BP 10) and mounted below the recording chamber, was used to present temporally-modulated, full-field light stimuli (approx. 2 mm in diameter) to the retinal slices. Ca^{2+} recordings were performed with a constant background illumination of 10^4 P*s^{-1} (photo-isomerization rate) for at least 15 seconds. Light stimuli consisted of a series of 1-second bright flashes with 4-second intervals. Flashes evoked similar photo-isomerization rates in both medium (M-) and short (S-)

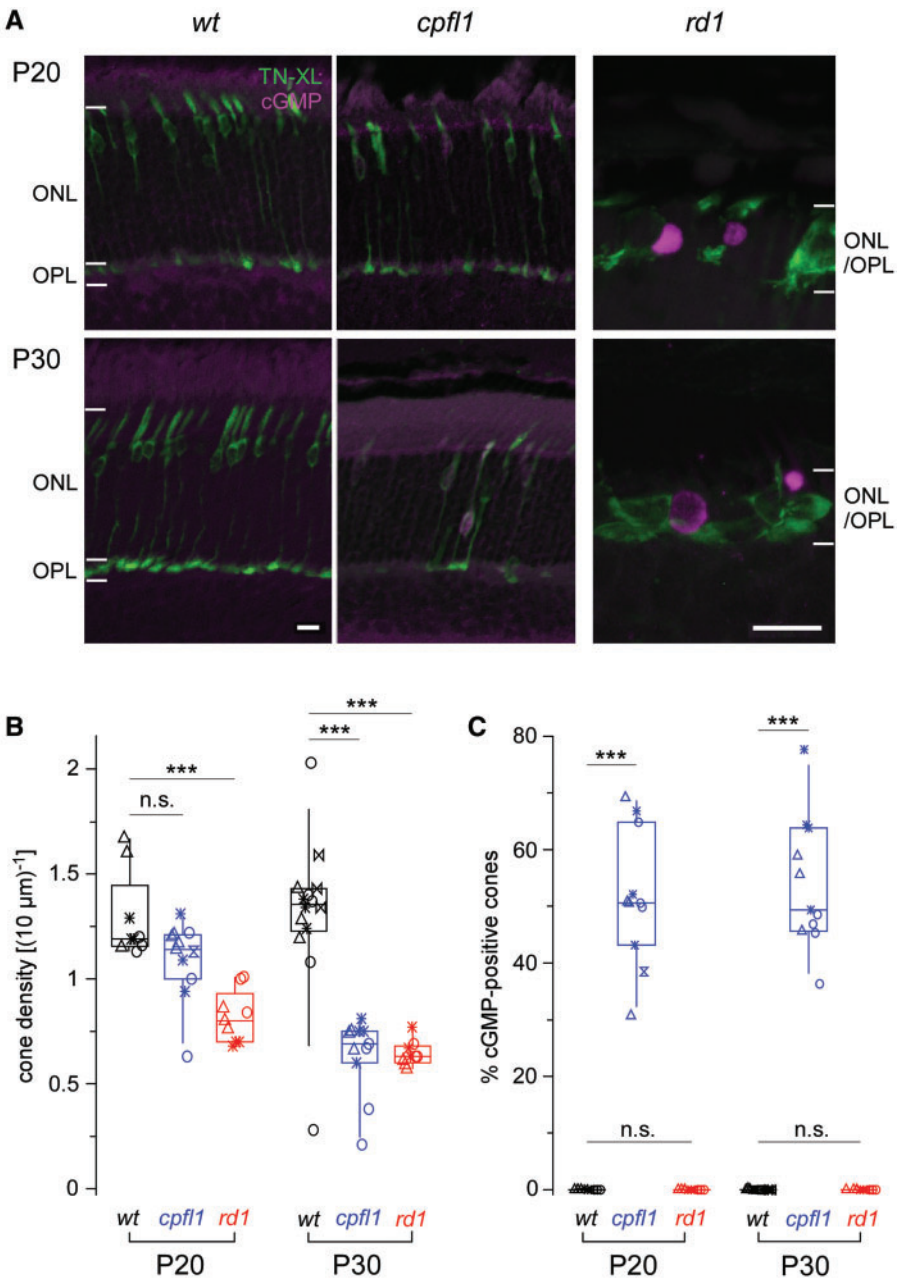

Figure 2. cGMP accumulation in photoreceptors of *Pde6* mutant mice expressing the *HR2.1:TN-XL* Ca^{2+}-biosensor. (**A**) Cross-sections of *wt* (left), *cpfl1* (centre), and *rd1* (right) outer retinas immunostained for cGMP (magenta) at P20 (top) and P30 (bottom). The biosensor TN-XL is shown in green. (**B**) Cone density (in # cells/10 μm) in *rd1* animals is significantly reduced at P20, while at P30 both *cpfl1* and *rd1* retinas show cone loss. (**C**) The percentage of cGMP-positive cones is strongly increased in *cpfl1* retina at P20 and P30, while *wt* and *rd1* cones are negative for cGMP. Scale bars: a, 10 µm. P20 data obtained from 9 sections from 3 *wt* mice (9/3); *cpfl1*, 11/3; *rd1*, 9/3; P30: *wt*, 14/4; *cpfl1*, 11/3; *rd1*, 9/3); *** $=P < 0.001$. OPL, outer plexiform layer, ONL, outer nuclear layer.

wavelength-sensitive cones (green LED: 6.7; UV LED: 6.5). At these light levels, rods are expected to be saturated and, therefore, light-evoked responses should originate in cones and not in electrically coupled rods. To record Ca^{2+} levels and light-evoked Ca^{2+} responses in cone axon terminals, we captured image series (128 x 16 pixels at 31.25 Hz), aligned with the outer plexiform layer (OPL) and covering an area of ~75 x 10 µm on the slice (Fig. 1D). We recorded both fluorescence channels, as TN-XL allows ratiometric measurements *via* FRET between its fluorophores enhanced cyan fluorescent protein (eCFP, donor) and citrine (acceptor).

In a subset of experiments, absolute Ca^{2+} concentrations were measured using an "*ex-vivo* slice calibration" procedure (31). We recorded the fluorescence ratio (see *Analysis of Ca^{2+} imaging data*) first in a standard ACSF solution (R_{base}, see below and Fig. 1D), then in Ca^{2+}-free ACSF supplemented with ionomycin (5 µM) and EGTA (10 mM) to determine the minimum ratio (R_{min}), and finally in ACSF supplemented with ionomycin (5 µM) and high Ca^{2+} (2.5 mM) to determine the maximum (saturating) ratio (R_{max}). The absolute Ca^{2+} concentration was estimated using R_{min}, R_{max}, the donor fluorescence with a saturating Ca^{2+} level ($F_{D,\ Ca\text{-}bound}$) and under Ca^{2+}-free conditions

($F_{D,\ Ca\text{-}free}$), as well as the *in-vivo* dissociation constant ($K_d = 0.77$, see (43)) for TN-XL:

$$[Ca^{2+}] = K_d \frac{R - R_{min}}{R_{max} - R} \cdot \frac{F_{D,Ca-free}}{F_{D,Ca-bound}}$$

Analysis of Ca^{2+} imaging data

All Ca^{2+} data were analysed using custom scripts for IGOR Pro 6.3 (Wavemetrics). To extract cone Ca^{2+} signals, regions of interest (ROIs) were drawn manually around the cone terminals (Fig. 1D) and the pixels within ROIs were averaged for each image frame. An ROI placed outside the OPL was used to determine the baseline fluorescence in both detection channels for background subtraction. The relative Ca^{2+} level was then determined as the ratio (R) between acceptor and donor fluorescence (F_A/F_D) signals after background subtraction. For each ROI, stimulus trials were averaged and the mean trace was filtered (boxcar, 320 ms filter-width).

Relative resting Ca^{2+} level (R_{base}) was defined as the mean prior to the light flash (*cf*. Fig. 3A). Further, we quantified the area between the base line and light response ("response area", R_A), response amplitude (ΔR), response rise (t_{20-80}). The latter was determined by fitting a sigmoid to the response rise to determine the duration between the time points when 20% and 80% ΔR were reached. As a measure for the "slowness" of a light response, we determined a "response lag" (t_{lag}), which we defined as the duration between $t_{20\%}$ and t_{decay}, the time point when the Ca^{2+} level started to recover (= to increase). In addition, we quantified response noise (R_{noise}), defined as s.d. of the traces (trials) after subtracting the low pass-filtered mean response (*cf*. Fig. 6A).

Previous studies showed that during slicing, cells close to the surface might be mechanically damaged and show abnormal Ca^{2+} ratios (28). We tried to address this issue by recording from cones at least 20-50 μm in the slice and by excluding cones with unstable baseline and/or extreme noise level. We used the noise distribution of the *wt* P30+ dataset and determined from the histogram the noise level ($R_{noise,max}$) that excluded the 5% cones with the highest noise (95th percentile). Then, from all datasets we excluded cones with $R_{noise} > R_{noise,max}$ unless they displayed clear light responses ($R_A > 10\ R_{A,noise}$, with $R_{A,noise}$ defined as the s.d. over the whole 5-s trace times the trial duration).

To compare responsiveness to light stimuli between the different data sets, we categorized the cones into "responsive" and "non-responsive". To include only cones with robust light responses into the "responsive" category, we again used the *wt* P30+ dataset: We determined the value ($R_{A,50\%}$) that divided the R_A histogram (*cf*. Fig. 4C) into halves and defined the 50% cones with the larger R_A values as responsive. This $R_{A,50\%}$ was then applied to the other datasets. Note that cones for which the response curve could not be fitted (to determine timing parameters, see above) were not classified as "responsive", even if they fulfilled the $R_A > R_{A,50\%}$ criterion.

Statistics

In total, we analysed $n = 2{,}678$ (89% of 3,007 cells) *wt*, $n = 1{,}992$ (81% of 2,469 cells) *cpfl1*, and $n = 1{,}696$ (92% of 1,845 cells) *rd1* cones. To compare Ca^{2+} level distributions statistically, we fitted the distribution of R_{base} for each line and time point with a Gaussian that was convoluted with an exponential (ExpModGauss in IGOR Pro) and used R_{base} at the distribution peak to centre the histograms for comparison between data sets (Fig. 3B). R_{base} distributions were compared using the Kolmogorov-Smirnov test (K-S test, IGOR Pro) for an alpha level of 5%. To compare the light response sizes statistically, we first normalized R_A of the responsive cells for all the datasets to the mean R_A of *wt* cones at P30+. To compare noise levels, we normalized R_{noise} measured in the mutant lines and at other time windows to $R_{noise,max}$ (see above). The Wilcoxon rank-sum test (as implemented in IGOR Pro; 5% alpha level) was used to compare R_A, t_{lag}, and R_{noise} between mouse lines and time windows. These data are shown as box-and-whisker plots (top whisker: 90th percentile; bottom whisker: 10th percentile).

Results

Normal *wt* cones and Ca^{2+} biosensor-expressing *wt* cones were previously found to be functionally equivalent, showing no differences in electroretinographic (ERG) recordings and opsin expression (28–30). To ascertain that the expression of the genetically encoded Ca^{2+} sensor TN-XL in mutant photoreceptors would not alter the degeneration phenotype, we first assessed degeneration markers in *HR2.1:TN-XL* crossbred mutants. For our analysis, we focussed on two time-windows, postnatal days (P) 18-20 and P30-33, to which we refer to as P18+ and P30+, respectively. In both *rd1* and *cpfl1* genotypes, these two periods correspond to times just beyond the onset of cone degeneration (P18+) and when roughly 50% of all cones are gone (P30+) (3,44).

Presence of biosensor does not alter *Pde6* mutant phenotype

Cone morphology in the *wt HR2.1:TN-XL* retina (control) appeared normal, whereas *HR2.1:TN-XL* x *cpfl1* cones were characterized by misplaced somata (Fig. 2A), as described before for non-biosensor *cpfl1* cones (3). Due to primary rod loss, *HR2.1:TN-XL* x *rd1* retina showed a marked thinning of the outer nuclear layer (ONL) (45), accompanied by dramatic changes in cone morphology (rounded somata with strongly altered neurite morphology; Fig. 2A), virtually identical to what has been described in the (non-biosensor) *rd1* mouse (5). We counted cones in the three mouse lines and found cone densities to be significantly reduced over time in *HR2.1:TN-XL* x *cpfl1* and *HR2.1:TN-XL* x *rd1* (Fig. 2B), indicating severe cone degeneration compared to *wt HR2.1:TN-XL*. Cone densities were within the ranges reported for non-biosensor *cpfl1* and *rd1* (Table 1). In addition, we performed TUNEL assays to evaluate the number of dying cells at P20 and P30 (Supplementary Material, Fig. S2) and found the fraction of TUNEL-positive cells in *HR2.1:TN-XL* x *cpfl1* and *HR2.1:TN-XL x rd1* lines to be similar to that reported for *cpfl1* and *rd1* before, respectively (Table 1) (3,38).

Next, we assessed cGMP accumulation in the outer retina (3,15): In *wild-type* retina, whether expressing the TN-XL biosensor or not, essentially no cGMP accumulation could be observed in the ONL, at P20 and P30 (Fig. 2A and C) (3). In *rd1* retina, the overall percentage of cGMP positive cells in the ONL at P20 was similar for biosensor and non-biosensor expressing retina (*rd1*: 7.44 ± 1.09% SD, $n = 9$ vertical sections from 3 mice; *HR2.1:TN-XL* x *rd1*: 6.91 ± 0.91% SD, $P = 0.5$, $n = 9$ vertical sections from 3 mice) and all available evidence suggests that this cGMP accumulation is restricted to rods exclusively. Since degenerating cones may lose the expression of conventional markers during

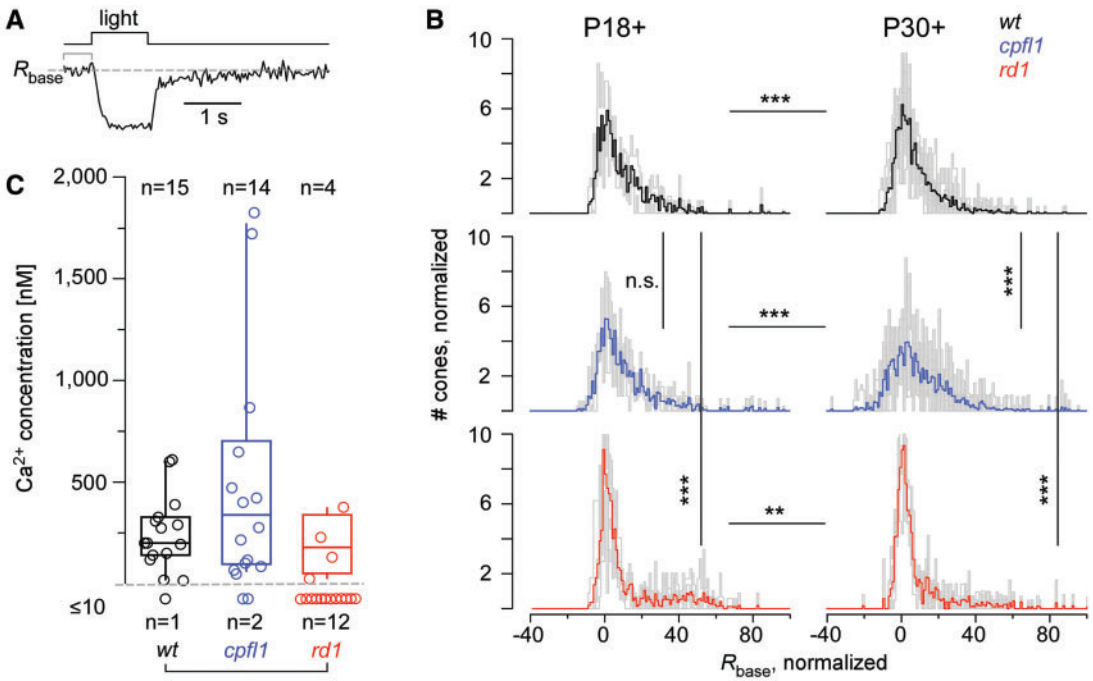

Figure 3. Cone resting Ca^{2+} levels. (**A**) Resting Ca^{2+} level (R_{base}) was determined as the mean trace prior to light flash. (**B**) Distribution of relative cone R_{base} in the three mouse lines at P18+ (left; *wt*, 853 cells from 3 mice (853/3); *cpfl1*, 944/4; *rd1*, 878/5) and P30+ (right; *wt*, 1,825/8; *cpfl1*, 1,048/8; *rd1*, 818/5; thick outline, mean distribution across mice; grey outlines, distributions from individual mice). Distributions were statistically compared using the K-S test (5% alpha level; $^{**}P < 0.01$; $^{***}P < 0.001$; n.s. 0.37). (**C**) Box-and-whisker plot of estimated absolute cone Ca^{2+} concentrations at P30+ for the three lines (*wt*, 16/2; *cpfl1*, 16/4; *rd1*, 16/3). Data points ≤ 10 nM were considered to represent unrealistically low Ca^{2+} levels (possibly due to a limitation of TN-XL, as discussed in (28)) and were thus excluded from the analysis.

the final stages of cell death, in non-biosensor *rd1* retina there is a degree of uncertainty as to whether *rd1* cones do show cGMP accumulation or not. However, in *HR2.1:TN-XL* x *rd1* retina, no cGMP positive cones could be detected, indicating that *rd1* cGMP accumulation was indeed restricted to rods only (Fig. 2A and C). In non-biosensor *cpfl1* retina, approximately 50% of the cones were positive for cGMP (3,15), similar to what was found in *HR2.1:TN-XL x cpfl1* cones (Fig. 2C).

In summary, we did not find any significant differences between the cones of the TN-XL biosensor-expressing and "normal" *rd1* and *cpfl1* mutants, suggesting that the mutant lines crossbred with *HR2.1:TN-XL* strain are suitable models to study cone function in health and disease. In addition, we showed that cGMP levels are strongly elevated in *cpfl1* but not in *rd1* cones. In the following, we will be addressing results obtained from the TN-XL expressing animals and, for ease of use, refer to these simply as *wt* (wild-type), *rd1*, and *cpfl1*.

Resting Ca^{2+} is very heterogeneous within cone populations and differs between mutants

To evaluate potential differences in Ca^{2+} homeostasis between mutant and *wt* lines, we recorded Ca^{2+} levels from TN-XL-expressing cones in acute vertical retinal slices using two-photon Ca^{2+} imaging (Fig. 1C and D; see Methods). We first assessed relative resting Ca^{2+} (R_{base}; Fig. 3A) and found that at the beginning of cone degeneration, at P18+, resting Ca^{2+} level distributions were comparable in *wt* and *cpfl1*, whereas the distribution for *rd1* was more narrow (Fig. 3B, *left column*). At P30+, when cone degeneration had progressed, the Ca^{2+} level distribution in *rd1* remained narrow, whereas the distributions for both *wt* and *cpfl1* broadened (Fig. 3B, *right column*). As some broadening was also observed in the *wt*, it may partially reflect developmental changes. Despite this, the effect was more pronounced in *cpfl1*. Taken together, these data suggest that the mutations in *cpfl1* and *rd1* have opposite effects on cone Ca^{2+} resting levels: As the degeneration progressed, *cpfl1* cone Ca^{2+} levels became increasingly heterogeneous, whereas *rd1* cone Ca^{2+} levels were (and remained) more homogenous across the population.

In a subset of experiments ($n = 9$ slices from 9 mice), we estimated the absolute resting Ca^{2+} concentrations in cones using an *ex-vivo* calibration approach in retinal slices (31,46). Because the difference in relative Ca^{2+} level distribution between *wt* and the two mutants was more prominent at P30+, we performed the calibration experiments at this age window. In *wt* cones, we determined an absolute cone Ca^{2+} concentration of 200 nM (median; $n = 15$ cones in 2 slices from 2 mice), which is in agreement with the literature (35,47). In *cpfl1* cones, the Ca^{2+} concentration was 339 nM ($n = 14$ cones in 4 slices from 4 mice), with a higher variability compared to *wt* (Fig. 3C). While these differences were not statistically significant, the higher variability in *cpfl1* Ca^{2+} concentration was consistent with the results from the relative Ca^{2+} distributions (Fig. 3B). Because of the low number of remaining cones in the *rd1* retina at P30+, we could only get a rough estimate for the absolute Ca^{2+} level in *rd1* cones (180 nM; $n = 4$ cones in 3 slices from 3 mice; Fig. 3C). However, since most Ca^{2+} values in *rd1* cones were below the detection limit of the TN-XL biosensor, the actual intracellular Ca^{2+} levels in *rd1* cones are likely to be much lower, similar to those measured under Ca^{2+}-free conditions.

Unexpected, robust light evoked Ca^{2+} responses in *cpfl1* cones

Previous ERG studies have reported very weak responses of *cpfl1* retina to bright-field light flashes but could not pinpoint the

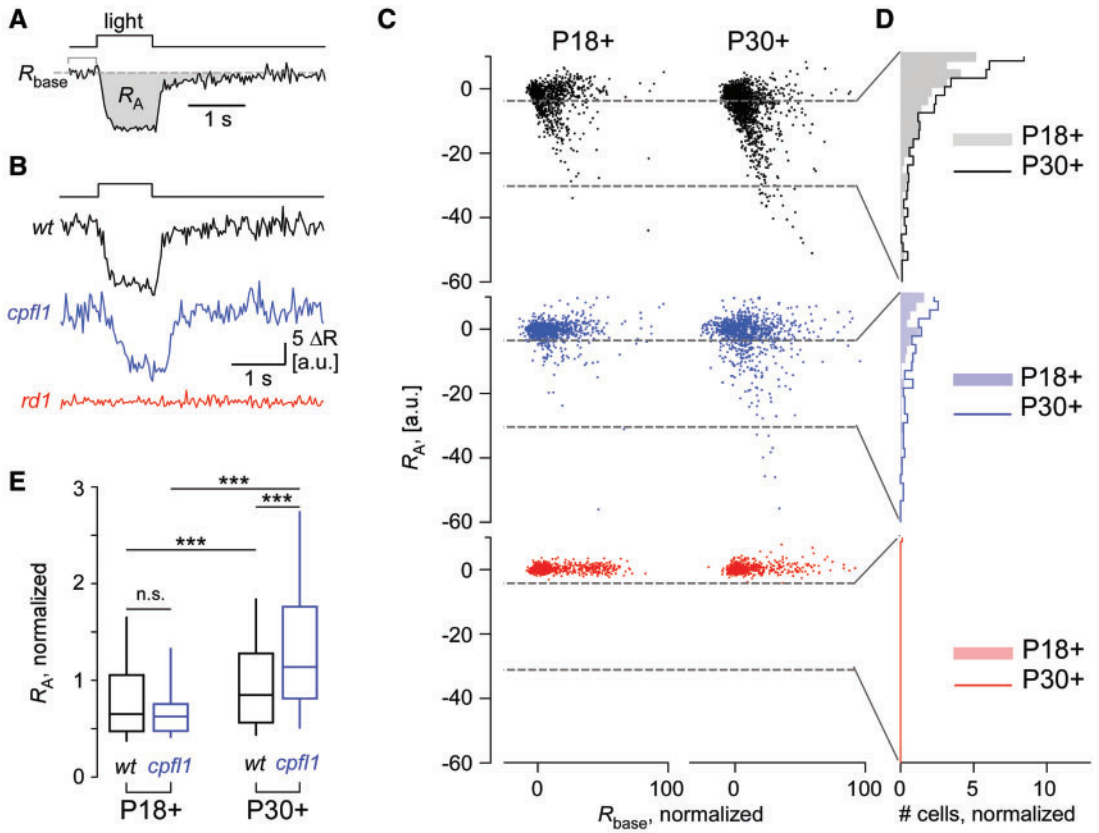

Figure 4. Light-evoked cone Ca^{2+} responses. (**A**) Determining area under the response curve (R_A) and relative resting Ca^{2+} level (R_{base}). (**B**) Exemplary Ca^{2+} signals (mean of ≥ 10 trials) in response to a light flash recorded from individual *wt* (black), *cpfl1* (blue), and *rd1* (red) cones at P30+. (**C**) R_A as function of R_{base} at P18+ (left) and P30+ (right). Each dot represents a single cone (colours as in B; P18+: *wt*, 853 from 3 mice (853/3); *cpfl1*, 944/4; *rd1*, 878/5; P30+: *wt*, 1,825/8; *cpfl1*, 1,048/8; *rd1*, 818/5). (**D**) Distribution of R_A in "responsive" cones (for definition, see Methods); only data points between the two dashed lines in (C) were included (colours as in b). (**E**) Box-and-whisker plot of normalized R_A at P18+ and P30+. At P18+, *wt*: 0.65 (median) (black, 160/3), *cpfl1*: 0.62 (blue, 32/4). At P30+, *wt*: 0.84, (730/8), *cpfl1*: 1.13, (99/8). R_A values were statistically compared using the Wilcoxon rank-sum test (5% alpha level; ***$P < 0.001$; n.s. $P = 0.47$).

Table 1. Cone density and percentage of TUNEL-positive cells in the studied mouse lines

	cone density[$(10\ \mu m)^{-1}$]		TUNEL positive cells[%]	
	P20	P30	P20	P30
"wild-type" HR2.1:TN-XL	1.28 (1.19)	1.31 (1.35)	0.17 (0.14)	0.03 (0.03)
HR2.1:TN-XL x cpfl1	1.09 (1.14)	0.63 (0.69)	0.32 (0.38)	0.17 (0.17)
HR2.1:TN-XL x rd1	0.81 (0.80)	0.64 (0.63)	2.51 (2.77)	0.76 (0.84)
wt	1.4 [P21] [61]	1.4 [61]	0.08 [15]	0.04 [15]
cpfl1	1.12 (1.13) [P24]	0.7 [†, 61]	0.15 [15]	0.02 [15]
rd1	0.75 [62]	0.60 [61]	1.64 [15]	0.55 [P28] [15]

For calculation of cone density and % TUNEL positive cells, see Methods. To allow for a comparison with earlier literature, values shown in this table are expressed as mean, with median (where available) in parenthesis. In cases where P20/P30 values were not available for comparison, the actual postnatal age is given in square brackets. *cpfl1* at P24: median 1.13 ± 0.18 SD, 14 vertical sections from 5 mice.

[†]value given ("50% of *wt*") was estimated using data given in [61]. References in superscript brackets.

origin of these responses (2). To test whether *cpfl1* cones respond to light, we recorded cone Ca^{2+} signals and presented 1-s full-field light flashes on a constant background (*cf.* Fig. 1D). In *wt* cones, a light-evoked a decrease in the fluorescence ratio (F_A/F_D) indicates a decrease in Ca^{2+} level due to a light-induced hyperpolarization of the cone (Fig. 4A). To quantify Ca^{2+} response sizes, we determined the response area (R_A). Light-evoked Ca^{2+} responses were detected in *wt*, and to our surprise, also in *cpfl1* cones but not in *rd1* cones (Fig. 4B). In general, response size tended to increase as resting Ca^{2+} levels rose.

As expected, we found the highest percentage of cones that met our conservative "responsiveness" criterion (Methods) in *wt* retina. The percentage of responsive *wt* cones increased from ~36% at P18+ to ~50% at P30+, (Fig. 4C and D), possibly due to postnatal maturation of mouse retina (48,49). In *cpfl1* retina, we found a substantial percentage of cones that displayed light responses comparable to those measured in *wt*. At P18+, ~8% of the recorded *cpfl1* cones were responsive; later this fraction increased to ~21%. Moreover, the response size dramatically increased in *cpfl1* cones at P30+ (Fig. 4E). Remarkably, at this stage

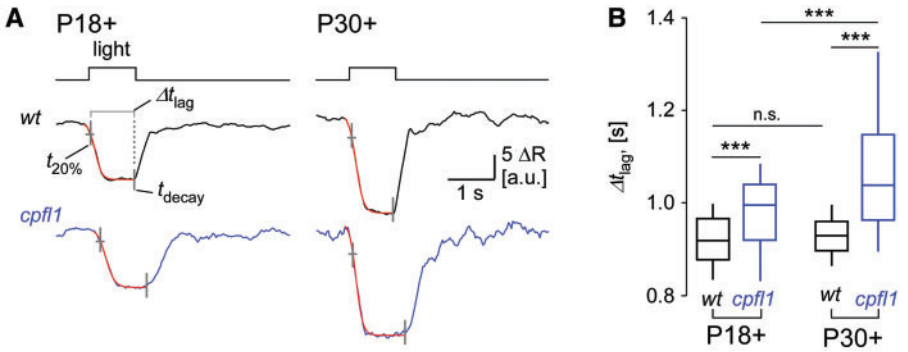

Figure 5. Kinetics of light-evoked Ca^{2+} responses in *wt* and *cpfl1* cones. (**A**) Exemplary light-evoked Ca^{2+} responses (means of ≥ 10 trials; smoothed using box-car, 320 ms filter-width) at P18+ and P30+ from *wt* (black) and *cpfl1* (blue). Response lag time (Δt_{lag}) was determined as the time between 20% of response rise ($t_{20\%}$) and beginning of response recovery (t_{decay}). (**B**) Box-and-whisker plot for Δt_{lag} for 1-s light flashes. At P18+, *wt*: 0.91 (median), (160 cones from 3 mice (160/3)); *cpfl1*: 0.99, (32/4). At P30+, *wt*: 0.93, (730/8), *cpfl1*: 1.03, (99/8). Δt_{lag} were statistically compared using the Wilcoxon rank-sum test (5% alpha level; *** $P < 0.001$; n.s. $P = 0.051$).

of *cpfl1* degeneration, about half of the cones were already lost. In comparison, in the secondary cone degeneration model *rd1*, where cones are genetically intact, less than 1% of the recorded cones were responsive.

Next, we wanted to see if the light-evoked Ca^{2+} response recorded in *cpfl1* cones differed from those in *wt* cones. Here, we focused on response kinetics, as responses appeared "slower" in *cpfl1* compared to *wt* (*cf.* Fig. 4B). First, we determined the "response lag" (Δt_{lag}) defined as the time period between the time when 20% of the response amplitude was reached ($t_{20\%}$) and the time when the Ca^{2+} level started to recover for a 1-s stimulus (t_{decay}; Fig. 5A). We found that Δt_{lag} was significantly longer in *cpfl1* than in *wt* cones at both ages (Fig. 5B). Moreover, Δt_{lag} in *cpfl1* cone responses increased significantly between P18+ and P30+. Taken together, our data suggest that even at P30+, a substantial fraction of *cpfl1* cones generate large, although sluggish light-evoked responses.

Cpfl1 cones are noisier than *wt* and *rd1* cones

We noticed that Ca^{2+} traces recorded in *cpfl1* cones appeared noisier compared to those in *wt* cones (Fig. 6A and B). This noise may reflect higher (spontaneous) activity caused by fluctuations in cGMP levels, possibly related to the cGMP accumulation we detected in *cpfl1* cones (50) (*cf.* Fig. 2A). To include *rd1* cones in this comparison, we analysed light-responsive and non-responsive cones separately (Fig. 6C and D). At P18+, noise levels were not significantly different between responsive *cpfl1* and *wt* cones, whereas non-responsive *cpfl1* cones were noisier than their *wt* counterparts. At P30+, both responsive and non-responsive *wt* cones became noisier, but much less so than *cpfl1*. The dramatic increase in Ca^{2+} signal noise recorded in *cpfl1* cones may indicate that cGMP fluctuations progressively increased in responsive cones. In contrast, *rd1* cones showed significantly lower noise than *wt* in both time windows. The small increase in *rd1* cone noise at P30+ may relate to the remodelling of the outer retina connectivity (5). In fact, this notion is supported by a study showing that the oscillatory activity that arises in the outer *rd1* retina (P30 and later) at least partially depends on voltage-gated Ca^{2+} channel activity in cone terminals (45).

Discussion

In many inherited retinal diseases, mutations that affect the photoreceptor OS lead to cell death, and the pathways associated with this are often linked to aberrant Ca^{2+} signalling. Here, we monitored Ca^{2+} dynamics directly during both primary and secondary cone degeneration, to show that Ca^{2+} signalling was indeed altered. Remarkably, although *cpfl1* cones suffer from primary *Pde6c* mutations, a subpopulation was found to be functional, while genetically intact *rd1* cones were entirely dysfunctional. Our results raise new questions as to the possible involvement of Ca^{2+} noise and random fluctuations, which could explain the stochastic nature of cone cell death (51–53). In addition, our study highlights the importance of using *in vivo* single-cell imaging techniques to improve our understanding of the intracellular processes leading to retinal degeneration.

Cone Ca^{2+} dynamics are altered in primary cone degeneration

Cpfl1 cones carry *Pde6c* mutations (1), exhibit cGMP accumulation, and are expected to show altered Ca^{2+} homeostasis (3,16). In line with previous studies, we found that the percentage of cones showing cGMP accumulation remained constant between P20 and P30. High cGMP is predicted to cause changes in Ca^{2+} homeostasis, as evidenced indirectly by the increased activity of Ca^{2+}-dependent calpain-type proteases (3,15). Our study confirms this prediction: Compared to *wt*, we found that *cpfl1* cones showed higher relative resting Ca^{2+} levels. In line with this, we found in our calibration experiments that *cpfl1* cones tended to have elevated absolute Ca^{2+} concentrations. In addition, *cpfl1* cones had larger light responses, their resting Ca^{2+} was much more heterogeneous, and they displayed increased Ca^{2+} noise levels. Overall, our results on primary *cpfl1* cone degeneration support the high Ca^{2+} hypothesis.

These results are interesting in the context of previous studies aimed at developing treatments for hereditary retinal degeneration. The use of inhibitors of the synaptic L-type VGCCs induced a delay in *rd1* photoreceptor degeneration (21), which implied that photoreceptor Ca^{2+} overload (16) would occur primarily *via* the synaptic axon terminal. We show that Ca^{2+} levels in the axon terminals of PDE6 mutant cones may indeed be increased; however, these changes are tightly linked to primary alterations of Ca^{2+} in the cone OS, as evidenced by our light stimulation experiments. Thus, when therapeutic strategies aimed at blocking either Ca^{2+}-permeable channels in the synapse (*i.e.* VGCCs) or in the OS (*i.e.* CNG-gated channels) (38,54) are compared, the latter appear to be a more suitable target.

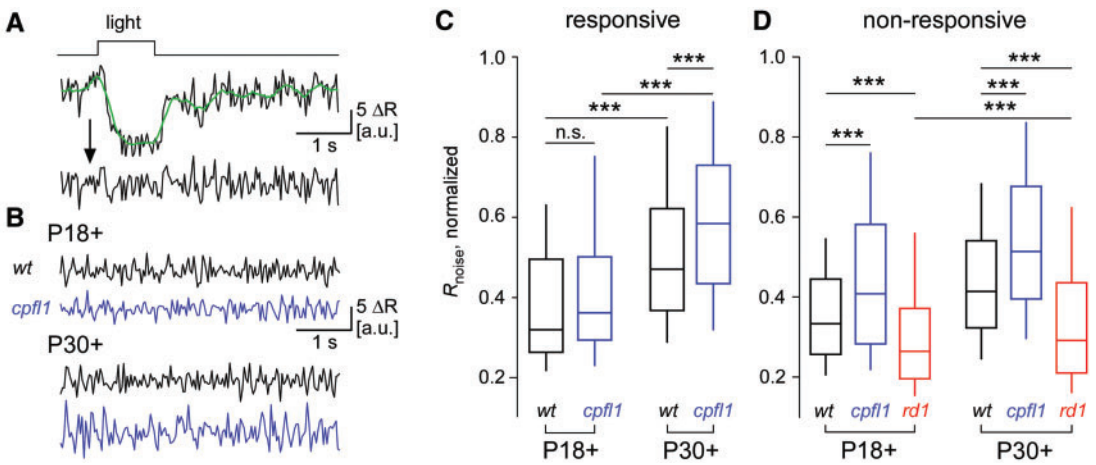

Figure 6. Ca^{2+} noise levels in cones. (**A**) Exemplary of Ca^{2+} response to a 1-s light flash (top, black trace). Noise was determined from traces with the low-pass filtered response (top, green trace; box-car, 320 ms filter-width) subtracted (bottom). (**B**) Exemplary noise traces at P18+ (top) and P30+ (bottom) from *wt* (black) and *cpfl1* (blue) cones. (**C**) Box-and-whisker plot of normalized noise (R_{noise}) for responsive *wt* and *cpfl1* cones at P18+ and P30+. At P18+, *wt*: 0.31 (median) (160 cones from three mice, 160/3), *cpfl1*: 0.36 (32/4). At P30+, *wt*: 0.47 (730/8), *cpfl1*: 0.59 (99/8). (**D**) Box-and-whisker plot of normalized R_{noise} for non-responsive *wt*, *cpfl1*, and *rd1* cones at P18+ and P30+. At P18+, *wt*: 0.33 (597/3), *cpfl1*: 0.40 (870/4), *rd1*: 0.26 (877/5). At P30+, *wt*: 0.41 (894/8), *cpfl1*: 0.51 (841/8), *rd1*: 0.29 (816/5). R_{noise} values were statistically compared using the Wilcoxon rank-sum test (5% alpha level; $^{***}P \leq 0.001$; n.s. $P = 0.10$).

Cone Ca^{2+} dynamics in secondary cone degeneration

In contrast to *cpfl1* cones, *rd1* cones are genetically intact and did not show cGMP accumulation. Yet, major cone loss was evident already at P20, progressing rapidly at P30. In *rd1*, cone OS and overall morphology changed dramatically in the absence of supporting rods as the photoreceptor layer thinned out. In addition, virtually no *rd1* cone responded to light, in line with previous ERG studies (23,38,54–56).

In this scenario, a modulation of cone terminal Ca^{2+} *via* the OS seems questionable. The resting Ca^{2+} distribution in the *rd1* cone population was significantly different at both P18+ and P30+ compared to *wt*, and *rd1* cone noise levels were significantly lower at both time points. When Ca^{2+} was washed out of *rd1* cones using ionomycin, the resting Ca^{2+} levels hardly changed at all. These results altogether point at a very low resting Ca^{2+} in cones upon loss of rods and structural disruption of the outer retina, indicating that *rd1* secondary cone cell death may be caused by exceedingly low Ca^{2+} levels ((57); discussed in (11,27)). This conclusion would have important implications for therapeutic developments, which often aim at lowering intracellular Ca^{2+}. While such an approach may be viable for primary cone degeneration (see above) it could be detrimental in secondary cone degeneration. To better understand Ca^{2+} dynamics in secondary cone degeneration, it may be necessary to study further animal models that exhibit a slower cone loss, not overlapping with postnatal retinal development, such as the *Pde6b*-mutant *rd10* mouse (4,15).

Cpfl1 cones show light evoked responses

To our surprise, a substantial number of *cpfl1* cones responded to light stimulation. These Ca^{2+} responses were larger and slower compared with *wt* cones, possibly due to low remnant PDE activity. Interestingly, cones treated with the PDE6 inhibitor zaprinast exhibited similar changes in response time course (28). Zaprinast application also caused a (reversible) increase in resting Ca^{2+}, consistent with our finding of higher absolute Ca^{2+} in *cpfl1* cones. The *cpfl1* allele carries two different mutations, one 116bp intronic insertion between exons 4 and 5 resulting in a splice defect, and one 1bp deletion resulting in a frameshift in exon 7 (1). These two mutations together are expected to abolish PDE6C function completely. Nevertheless, a small proportion of correctly spliced *Pde6c* transcript carrying only the 1bp deletion appears to be present in *cpfl1* cones (1), suggesting that they express lower amounts of PDE6C protein. Due to the severity of the genetic damage, it is unlikely, however, that this protein is functional. On the other hand, *cpfl1* mice do show weak responses in photopic ERG recordings (2). Here, a possible explanation is that *cpfl1* cones recruit low levels of rod *Pde6a*, which would be expected to slow-down cone response kinetics (58), similar to what we observed. Irrespective of the underlying mechanism, our results show that *cpfl1* mice do have a residual cone function at least until one month postnatal.

Degenerating cones show altered noise levels

In *wt* cones, Ca^{2+} noise levels became significantly higher from P18+ to P30+, suggesting changes in PDE/cGMP/Ca^{2+} signalling with time, as the development and maturation of cones and retinal circuitry progresses (48). Previous studies have found that cone noise depends on variations in CNG channel activity and fluctuations in cGMP levels in the OS (50,59). Moreover, cone noise persists in the downstream circuitry (60).

Our data show altered Ca^{2+} noise levels in both primary and secondary cone degeneration. At P30+, in both responsive and non-responsive *cpfl1* cones, Ca^{2+} noise was significantly higher than in their *wt* counterparts, possibly due to the higher overall Ca^{2+} levels in *cpfl1* cones. It is tempting to speculate that such variations in Ca^{2+} noise (or Ca^{2+} fluctuations above or below a critical threshold) over time could contribute to the stochastic nature of photoreceptor cell death. Although at the tissue level, photoreceptor degeneration appears as a well-timed process, the time point when cell death is initiated at the level of the individual photoreceptor is random; it is inherently impossible to predict when a specific photoreceptor is going to die (51–53).

The precise processes that may be triggered by Ca^{2+} fluctuations remain unknown, but could potentially be linked to activation of Ca^{2+}-dependent kinases (61,62) with bearings on

gene expression (63) and/or Ca^{2+}-dependent calpain-type proteases (3,19). On the other hand, a recent *in vivo* Ca^{2+} imaging study followed degenerating cones over a time-course of several hours in intact zebrafish larvae carrying the *cpfl1*-like *Pde6c*^{w59} mutation and reported suppressed Ca^{2+} fluctuations when compared to *wt* (26). At present, it is unclear where these differences between mutant cones in zebrafish and mouse arise, but they could be related to developmental stage, experimental conditions, and perhaps species differences. Ca^{2+} fluctuations may have either beneficial or detrimental consequences. In *rd1* cones, on the other hand, Ca^{2+} noise was significantly lower than in *wt*, most likely because of the lower Ca^{2+} baseline levels. An exciting topic for future studies will be to understand if and how increased Ca^{2+} noise or overall changes in Ca^{2+} signalling contribute to these degenerative events.

Concluding remarks and future aspects

Several investigations were based on the assumption that altered Ca^{2+} signalling is involved in or serves as a trigger for rod and cone degeneration (*e.g.* (21,54,64)). Our results indeed show alterations in the dynamics of Ca^{2+} signalling in both primary and secondary cone degeneration. For primary cone degeneration, our data is in line with the "high Ca^{2+} hypothesis", suggesting that cell death may be triggered by Ca^{2+} overload, possibly *via* higher random fluctuations in Ca^{2+} levels. This may have a bearing on the stochastics of cone degeneration (as discussed above) but still leaves open the question whether changes in Ca^{2+} and/or Ca^{2+}-dependent enzymes are cause or consequence of primary cone degeneration. Secondary cone degeneration, on the other hand, is very likely associated with low Ca^{2+} levels and is, thus, more consistent with the "low Ca^{2+} hypothesis". This may also be true for primary photoreceptor degeneration triggered by mutations that cause low Ca^{2+} (*e.g.* CNG channel mutations). Taken together, these findings may have important ramifications for therapeutic approaches focusing on blocking Ca^{2+} influx in hereditary retinal degeneration. Here, our study may help to reconcile both the high and low Ca^{2+} hypotheses (16,27) and contribute to resolving a long-lasting controversy on the use of Ca^{2+} channel antagonists for the treatment of inherited retinal degeneration (21–23).

To gain insight into the precise timing and the role of Ca^{2+} signalling in the execution of cell death, Ca^{2+} imaging experiments will need to be combined with cellular activity assays for Ca^{2+} targets such as kinases, proteases, or histone deacetylases (65,66). On a different note, our study also showed that even genetically impaired cones may show considerable functional activity, highlighting the importance of Ca^{2+} measurements at single-cell resolution to obtain direct readouts on the functionality and health of cones.

Supplementary Material

Supplementary Material is available at *HMG* online.

Acknowledgements

We thank Gordon Eske, Norman Rieger, and Klaudija Masarini for technical assistance; Simone De Giovanni, Christian Behrens, and Philipp Berens for helpful discussions; Ayse Sahaboglu-Tekgoez, and Robin Kemmler for technical advice and discussions.

Conflict of Interest statement. None declared.

Funding

This work was supported by the Deutsche Forschungsgemeinschaft (DFG) (Werner Reichardt Centre for Integrative Neuroscience Tübingen, EXC 307 to TE; EU 42/8-1 to TE; KFO 134 and PA 1751/7-1 to FPD; TR 1238/4-1 to DT), fortüne to TE, Neuro-Ophthalmologische Gesellschaft to TE, and the European Union (DRUGSFORD; HEALTH-F2-2012-304963 to FPD).

References

1. Chang, B., Grau, T., Dangel, S., Hurd, R., Jurklies, B., Sener, E.C., Andreasson, S., Dollfus, H., Baumann, B., Bolz, S., *et al.* (2009) A homologous genetic basis of the murine cpfl1 mutant and human achromatopsia linked to mutations in the PDE6C gene. *Proc. Natl. Acad. Sci. U. S. A*, **106**, 19581–19586.,
2. Schaeferhoff, K., Michalakis, S., Tanimoto, N., Fischer, M.D., Becirovic, E., Beck, S.C., Huber, G., Rieger, N., Riess, O., Wissinger, B., *et al.* (2010) Induction of STAT3-related genes in fast degenerating cone photoreceptors of cpfl1 mice. *Cell. Mol. Life Sci.*, **67**, 3173–3186.
3. Trifunović, D., Dengler, K., Michalakis, S., Zrenner, E., Wissinger, B. and Paquet-Durand, F. (2010) cGMP-dependent cone photoreceptor degeneration in the cpfl1 mouse retina. *J. Comp. Neurol.*, **518**, 3604–3617.
4. Gargini, C., Terzibasi, E., Mazzoni, F. and Strettoi, E. (2007) Retinal organization in the retinal degeneration 10 (rd10) mutant mouse: a morphological and ERG study. *J. Comp. Neurol.*, **500**, 222–238.
5. Lin, B., Masland, R.H. and Strettoi, E. (2009) Remodeling of cone photoreceptor cells after rod degeneration in rd mice. *Exp. Eye Res.*, **88**, 589–599.
6. Bowes, C., Li, T., Danciger, M., Baxter, L.C., Applebury, M.L. and Farber, D.B. (1990) Retinal degeneration in the rd mouse is caused by a defect in the beta subunit of rod cGMP-phosphodiesterase. *Nature*, **347**, 677–680.
7. Mercer, A.J. and Thoreson, W.B. (2011) The dynamic architecture of photoreceptor ribbon synapses: cytoskeletal, extracellular matrix, and intramembrane proteins. *Vis. Neurosci.*, **28**, 453–471.
8. Koch, K.W. and Dell'Orco, D. (2013) A calcium-relay mechanism in vertebrate phototransduction. *ACS Chem. Neurosci.*, **4**, 909–917.
9. Schmitz, F. (2014) Presynaptic [Ca(2+)] and GCAPs: aspects on the structure and function of photoreceptor ribbon synapses. *Front. Mol. Neurosci.*, **7**, 3.
10. Koutalos, Y. and Yau, K.W. (1996) Regulation of sensitivity in vertebrate rod photoreceptors by calcium. *Trends Neurosci.*, **19**, 73–81.
11. Burns, M.E. and Arshavsky, V.Y. (2005) Beyond counting photons: trials and trends in vertebrate visual transduction. *Neuron*, **48**, 387–401.
12. Burns, M.E. and Pugh, E.N. (2010) Lessons from photoreceptors: turning off g-protein signaling in living cells. *Physiology (Bethesda).*, **25**, 72–84.
13. Farber, D.B. and Lolley, R.N. (1974) Cyclic guanosine monophosphate: elevation in degenerating photoreceptor cells of the C3H mouse retina. *Science.*, **186**, 449–451.
14. Paquet-Durand, F., Hauck, S.M., van Veen, T., Ueffing, M. and Ekström, P. (2009) PKG activity causes photoreceptor cell death in two retinitis pigmentosa models. *J. Neurochem.*, **108**, 796–810.
15. Arango-Gonzalez, B., Trifunović, D., Sahaboglu, A., Kranz, K., Michalakis, S., Farinelli, P., Koch, S., Koch, F., Cottet, S.,

Janssen-Bienhold, U., *et al*. (2014) Identification of a common non-apoptotic cell death mechanism in hereditary retinal degeneration. *PLoS One*, **9**, e112142.
16. Fox, D.A., Poblenz, A.T. and He, L. (1999) Calcium overload triggers rod photoreceptor apoptotic cell death in chemical-induced and inherited retinal degenerations. *Ann. N. Y. Acad. Sci.*, **893**, 282–285.
17. Olshevskaya, E.V., Calvert, P.D., Woodruff, M.L., Peshenko, I.V., Savchenko, A.B., Makino, C.L., Ho, Y.S., Fain, G.L. and Dizhoor, A.M. (2004) The Y99C mutation in guanylyl cyclase-activating protein 1 increases intracellular Ca2+ and causes photoreceptor degeneration in transgenic mice. *J. Neurosci.*, **24**, 6078–6085.
18. Doonan, F., Donovan, M. and Cotter, T.G. (2005) Activation of multiple pathways during photoreceptor apoptosis in the rd mouse. *Invest. Ophthalmol. Vis. Sci.*, **46**, 3530–3538.
19. Paquet-Durand, F., Azadi, S., Hauck, S.M., Ueffing, M., van Veen, T. and Ekström, P. (2006) Calpain is activated in degenerating photoreceptors in the rd1 mouse. *J. Neurochem.*, **96**, 802–814.
20. Sanges, D., Comitato, A., Tammaro, R. and Marigo, V. (2006) Apoptosis in retinal degeneration involves cross-talk between apoptosis-inducing factor (AIF) and caspase-12 and is blocked by calpain inhibitors. *Proc. Natl. Acad. Sci.*, **103**, 17366–17371.
21. Frasson, M., Sahel, J.A., Fabre, M., Simonutti, M., Dreyfus, H. and Picaud, S. (1999) Retinitis pigmentosa: rod photoreceptor rescue by a calcium-channel blocker in the rd mouse. *Nat. Med.*, **5**, 1183–1187.
22. Bush, R.A., Kononen, L., Machida, S. and Sieving, P.A. (2000) The effect of calcium channel blocker diltiazem on photoreceptor degeneration in the rhodopsin Pro213His rat. *Invest. Ophthalmol. Vis. Sci.*, **41**, 2697–2701.
23. Pawlyk, B.S., Li, T., Scimeca, M.S., Sandberg, M.A. and Berson, E.L. (2002) Absence of photoreceptor rescue with D-cis-diltiazem in the rd mouse. *Invest. Ophthalmol. Vis. Sci.*, **43**, 1912–1915.
24. Barabas, P., Cutler Peck, C. and Krizaj, D. (2010) Do calcium channel blockers rescue dying photoreceptors in the Pde6b (rd1) mouse? *Adv. Exp. Med. Biol.*, **664**, 491–499.
25. Xu, J., Morris, L., Thapa, A., Ma, H., Michalakis, S., Biel, M., Baehr, W., Peshenko, I.V., Dizhoor, A.M. and Ding, X.Q. (2013) cGMP accumulation causes photoreceptor degeneration in CNG channel deficiency: evidence of cGMP cytotoxicity independently of enhanced CNG channel function. *J. Neurosci.*, **33**, 14939–14948.
26. Ma, E.Y., Lewis, A., Barabas, P., Stearns, G., Suzuki, S., Krizaj, D. and Brockerhoff, S.E. (2013) Loss of Pde6 reduces cell body Ca(2+) transients within photoreceptors. *Cell Death Dis.*, **4**, e797.
27. Fain, G.L. and Lisman, J.E. (1999) Light, Ca2+, and photoreceptor death: new evidence for the equivalent-light hypothesis from arrestin knockout mice. *Invest. Ophthalmol. Vis. Sci.*, **40**, 2770–2772.
28. Wei, T., Schubert, T., Paquet-Durand, F., Tanimoto, N., Chang, L.L., Koeppen, K., Ott, T., Griesbeck, O., Seeliger, M.W., Euler, T., *et al*. (2012) Light-driven calcium signals in mouse cone photoreceptors. *J. Neurosci.*, **32**, 6981–6994.
29. Baden, T., Schubert, T., Chang, L., Wei, T., Zaichuk, M., Wissinger, B. and Euler, T. (2013) A Tale of Two Retinal Domains: Near-Optimal Sampling of Achromatic Contrasts in Natural Scenes through Asymmetric Photoreceptor Distribution. *Neuron*, **80**, 1206–1217.
30. Kemmler, R., Schultz, K., Dedek, K., Euler, T. and Schubert, T. (2014) Differential regulation of cone calcium signals by different horizontal cell feedback mechanisms in the mouse retina. *J. Neurosci.*, **34**, 11826–11843.
31. Kulkarni, M., Schubert, T., Baden, T., Wissinger, B., Euler, T. and Paquet-Durand, F. (2015) Imaging Ca2+ Dynamics in Cone Photoreceptor Axon Terminals of the Mouse Retina. *J. Vis. Exp.*, 10.3791/52588.
32. Heidelberger, R., Heinemann, C., Neher, E. and Matthews, G. (1994) Calcium dependence of the rate of exocytosis in a synaptic terminal. *Nature*, **371**, 513–515.
33. Rieke, F. and Schwartz, E.A. (1994) A cGMP-gated current can control exocytosis at cone synapses. *Neuron*, **13**, 863–873.
34. Choi, S.Y., Borghuis, B.G., Borghuis, B., Rea, R., Levitan, E.S., Sterling, P. and Kramer, R.H. (2005) Encoding light intensity by the cone photoreceptor synapse. *Neuron*, **48**, 555–562.
35. Choi, S.Y., Jackman, S., Thoreson, W.B. and Kramer, R.H. (2008) Light regulation of Ca2+ in the cone photoreceptor synaptic terminal. *Vis. Neurosci.*, **25**, 693–700.
36. Mank, M., Reiff, D.F., Heim, N., Friedrich, M.W., Borst, A. and Griesbeck, O. (2006) A FRET-based calcium biosensor with fast signal kinetics and high fluorescence change. *Biophys. J.*, **90**, 1790–1796.
37. Schubert, T., Gleiser, C., Heiduschka, P., Franz, C., Nagel-Wolfrum, K., Sahaboglu, A., Weisschuh, N., Eske, G., Rohbock, K., Rieger, N., *et al*. (2015) Deletion of myosin VI causes slow retinal optic neuropathy and age-related macular degeneration (AMD)-relevant retinal phenotype. *Cell. Mol. Life Sci.*, **72**, 3953–3969.,
38. Paquet-Durand, F., Beck, S., Michalakis, S., Goldmann, T., Huber, G., Mühlfriedel, R., Trifunović, D., Fischer, M.D., Fahl, E., Duetsch, G., *et al*. (2011) A key role for cyclic nucleotide gated (CNG) channels in cGMP-related retinitis pigmentosa. *Hum. Mol. Genet.*, **20**, 941–947.
39. Chang, B. (2015) Survey of the nob5 mutation in C3H substrains. *Mol. Vis.*, **21**, 1101–1105.
40. Pfeiffer-Guglielmi, B., Fleckenstein, B., Jung, G. and Hamprecht, B. (2003) Immunocytochemical localization of glycogen phosphorylase isozymes in rat nervous tissues by using isozyme-specific antibodies. *J. Neurochem.*, **85**, 73–81.
41. Werblin, F.S. (1978) Transmission along and between rods in the Tiger Salamander Retina. *J. Physiol.*, **280**, 449–470.
42. Euler, T., Hausselt, S.E., Margolis, D.J., Breuninger, T., Castell, X., Detwiler, P.B. and Denk, W. (2009) Eyecup scope–optical recordings of light stimulus-evoked fluorescence signals in the retina. *PflüGers Arch. Eur. J. Physiol.*, **457**, 1393–1414.
43. Hendel, T., Mank, M., Schnell, B., Griesbeck, O., Borst, A. and Reiff, D.F. (2008) Fluorescence changes of genetic calcium indicators and OGB-1 correlated with neural activity and calcium in vivo and in vitro. *J. Neurosci.*, **28**, 7399–7411.
44. Carter-Dawson, L.D., LaVail, M.M. and Sidman, R.L. (1978) Differential effect of the rd mutation on rods and cones in the mouse retina. *Investig. Ophthalmol. Vis. Sci.*, **17**, 489–498.
45. Haq, W., Arango-Gonzalez, B., Zrenner, E., Euler, T. and Schubert, T. (2014) Synaptic remodeling generates synchronous oscillations in the degenerated outer mouse retina. *Front. Neural Circuits*, **8**, 108.
46. Sheng, Z., Choi, S.Y., Dharia, A., Li, J., Sterling, P. and Kramer, R.H. (2007) Synaptic Ca2+ in darkness is lower in rods than cones, causing slower tonic release of vesicles. *J. Neurosci.*, **27**, 5033–5042.
47. Johnson, J.E., Perkins, G.A., Giddabasappa, A., Chaney, S., Xiao, W., White, A.D., Brown, J.M., Waggoner, J., Ellisman,

M.H. and Fox, D.A. (2007) Spatiotemporal regulation of ATP and Ca2+ dynamics in vertebrate rod and cone ribbon synapses. *Mol. Vis.*, **13**, 887–919.
48. Szél, A., Röhlich, P., Mieziewska, K., Aguirre, G. and van Veen, T. (1993) Spatial and temporal differences between the expression of short- and middle-wave sensitive cone pigments in the mouse retina: a developmental study. *J. Comp. Neurol.*, **331**, 564–577.
49. Gibson, R., Fletcher, E.L., Vingrys, A.J., Zhu, Y., Vessey, K.A. and Kalloniatis, M. (2013) Functional and neurochemical development in the normal and degenerating mouse retina. *J. Comp. Neurol.*, **521**, 1251–1267.
50. Angueyra, J.M. and Rieke, F. (2013) Origin and effect of phototransduction noise in primate cone photoreceptors. *Nat. Neurosci.*, **16**, 1692–1700.
51. Clarke, G., Collins, R.A., Leavitt, B.R., Andrews, D.F., Hayden, M.R., Lumsden, C.J. and McInnes, R.R. (2000) A one-hit model of cell death in inherited neuronal degenerations. *Nature*, **406**, 195–199.
52. Clarke, G., Lumsden, C.J. and McInnes, R.R. (2001) Inherited neurodegenerative diseases: the one-hit model of neurodegeneration. *Hum. Mol. Genet.*, **10**, 2269–2275.
53. Sahaboglu, A., Paquet-Durand, O., Dietter, J., Dengler, K., Bernhard-Kurz, S., Ekström, P.A., Hitzmann, B., Ueffing, M. and Paquet-Durand, F. (2013) Retinitis pigmentosa: rapid neurodegeneration is governed by slow cell death mechanisms. *Cell Death Dis.*, **4**, e488.
54. Read, D.S., McCall, M.A. and Gregg, R.G. (2002) Absence of voltage-dependent calcium channels delays photoreceptor degeneration in rd mice. *Exp. Eye Res.*, **75**, 415–420.,
55. Bonaventure, N., Wioland, N. and Karli, P. (1985) Enhanced sensory convergence to the visual cortex in the rodless (rd/rd) mouse. *Doc. Ophthalmol.*, **61**, 97–103.
56. Strettoi, E., Pignatelli, V., Rossi, C., Porciatti, V. and Falsini, B. (2003) Remodeling of second-order neurons in the retina of rd/rd mutant mice. *Vision Res.*, **43**, 867–877.
57. Woodruff, M.L., Wang, Z., Chung, H.Y., Redmond, T.M., Fain, G.L. and Lem, J. (2003) Spontaneous activity of opsin apoprotein is a cause of Leber congenital amaurosis. *Nat. Genet.*, **35**, 158–164.
58. Kolandaivelu, S., Chang, B. and Ramamurthy, V. (2011) Rod phosphodiesterase-6 (PDE6) catalytic subunits restore cone function in a mouse model lacking cone PDE6 catalytic subunit. *J. Biol. Chem.*, **286**, 33252–33259.
59. Holcman, D. and Korenbrot, J.I. (2005) The Limit of Photoreceptor Sensitivity: Molecular Mechanisms of Dark Noise in Retinal Cones. *J. Gen. Physiol.*, **125**, 641–660.
60. Ala-Laurila, P., Greschner, M., Chichilnisky, E.J. and Rieke, F. (2011) Cone photoreceptor contributions to noise and correlations in the retinal output. *Nat. Neurosci.*, **14**, 1309–1316.
61. Hauck, S.M., Ekström, P.A., Ahuja-Jensen, P., Suppmann, S., Paquet-Durand, F., van Veen, T. and Ueffing, M. (2006) Differential modification of phosducin protein in degenerating rd1 retina is associated with constitutively active Ca2+/calmodulin kinase II in rod outer segments. *Mol. Cell. Proteomics*, **5**, 324–336.
62. Azadi, S., Paquet-Durand, F., Medstrand, P., van Veen, T. and Ekström, P.A. (2006) Up-regulation and increased phosphorylation of protein kinase C (PKC) delta, mu and theta in the degenerating rd1 mouse retina. *Mol. Cell. Neurosci.*, **31**, 759–773.
63. Azadi, S., Johnson, L.E., Paquet-Durand, F., Perez, M.T.R., Zhang, Y., Ekström, P.A. and van Veen, T. (2007) CNTF+BDNF treatment and neuroprotective pathways in the rd1 mouse retina. *Brain Res.*, **1129**, 116–129.
64. Takano, Y., Ohguro, H., Dezawa, M., Ishikawa, H., Yamazaki, H., Ohguro, I., Mamiya, K., Metoki, T., Ishikawa, F. and Nakazawa, M. (2004) Study of drug effects of calcium channel blockers on retinal degeneration of rd mouse. *Biochem. Biophys. Res. Commun.*, **313**, 1015–1022.
65. Qiu, Z. and Ghosh, A. (2008) A calcium-dependent switch in a CREST-BRG1 complex regulates activity-dependent gene expression. *Neuron*, **60**, 775–787.
66. Tian, X., Gala, U., Zhang, Y., Shang, W., Nagarkar Jaiswal, S., di Ronza, A., Jaiswal, M., Yamamoto, S., Sandoval, H., Duraine, L., *et al.* (2015) A voltage-gated calcium channel regulates lysosomal fusion with endosomes and autophagosomes and is required for neuronal homeostasis. *PLoS Biol.*, **13**, e1002103.